Twenty-Sixth Symposium (International) on Combustion/The Combustion Institute, 1996/pp. 1453–1459

MEASUREMENTS AND PREDICTION OF AIR ENTRAINMENT RATES OF POOL FIRES

X. C. ZHOU AND JAYAVANT P. GORE
Thermal Sciences and Propulsion Center
School of Mechanical Engineering
Purdue University
W. Lafayette, IN 47907-1003, USA

HOWARD R. BAUM
Center for Fire Research
Building and Fire Research Laboratory
National Institute of Standards and Technology
Gaithersburg, MD 20899, USA

Motivated by the various applications of entrainment rate correlations in fire research and the large uncertainty in the efficacy of existing correlations and experimental data, the first particle imaging velocimetry (PIV)-based measurements of fire-induced flow field around pool fires burning methanol, heptane, and toluene were obtained. Air entrainment rates for 15-cm and 30-cm pool fires burning the three different fuels were calculated based on the mean velocity field. The entrainment data for the six fires could be correlated well using the fire Froude number as the nondimensional parameter. An existing kinematic approach to the prediction of the fire-induced flow field was extended to the present fires. The driving processes for the entrainment flow, namely, the volumetric heat release and the baroclinic vorticity generation, were evaluated based on correlations of buoyant diffusion flame structure in the literature. The predicted entrainment velocities were substantially higher than the measurements but were in qualitative agreement with the data. On this basis the heat release rate and vorticity correlations used in the analysis were corrected by using a smaller radius for the 1/*e* point in the velocity profile. The modified predictions were in better agreement with the experimental data. Therefore, further evaluation of the kinematic approach with proper heat release rate and vorticity distributions is warranted.

Introduction

Air entrainment influences the size and shape of a pool fire, its soot generation, and the combustion product composition. Motivated by this, many researchers have investigated air entrainment rates of buoyant diffusion flames [1–19]. Entrainment rate is defined as the change in the axial mass flow rate of air with distance from the fuel surface [1,3,10,20]. Some have used alternate definitions such as the rate of addition of air mass into visible flame interface or into an interface between the potential and vortical parts of the flow field [1,9–18]. The researchers measured entrainment rates using one of four experimental techniques [1,6,10–18,20]. The different measurement techniques led to explicit and implicit differences between the measured entrainment rates and those implied by the desired definition.

The first experimental technique for estimating entrainment rates involved measurements of axial velocity and temperature [4–9]. The investigators used the temperature data to calculate the density using the ideal gas equation, a constant thermodynamic pressure, and a constant estimated molecular weight. McCaffrey and co-workers and Cox and coworkers [4–6] used curve fits of density and velocity extending to a radial distance tending to infinity to calculate the axial flow rate and the entrainment rate. Cox and coworkers [5,6] found the density–velocity correlations to be important. Other researchers used the method for evaluating the axial mass flow with the radius of the visible flame boundary as the limiting value [7–9]. McCaffrey [4] observed that the two interfaces resulted in entrainment rates different by more than a factor of 2. In addition to the differences caused by the use of different radial locations, a difficulty in this procedure is the magnification of the large uncertainties in the velocity data at the farthest radial locations.

Ricou and Spalding [10] and Delichatsios and Orloff [11] obtained direct measurements of the mass flow rate of air needed for maintaining a mass balance in an enclosure surrounding the fire. The investigators stated that a judicious selection of the

TABLE 1
Operating conditions and global properties of the pool fires

D, cm	Fuel	H_f, cm	$\dot{m}_f$, mg/s	X_A, %	X_R, %	S	Fr
15	methanol	32	245	100	20	6.4	0.014
15	heptane	62	385	90	30	14.3	0.070
15	toluene	58	370	90	30	13.5	0.071
30	methanol	36	980	100	20	6.4	0.026
30	heptane	134	2660	90	30	14.3	0.088
30	toluene	119	2850	90	30	13.5	0.103

enclosure and the exit orifice diameter are necessary. The technique allowed much better correlations of forced jet entrainment-rate data [10] than those of buoyant diffusion flames [10,11], probably due to the higher sensitivity of buoyant fires to boundary conditions.

The third measurement technique involved sampling and gas chromatography of combustion products from a stably stratified layer. Zukoski and coworkers [12–15] used mass and species balance equations together with a knowledge of the fuel composition and stoichiometry to obtain the air entrainment rate. In a recent paper, Zukoski [16] expressed concern that the stable upper layer affects the entrainment flow field and hence that the resulting entrainment rate data should be considered to be specific for a particular interface height. The selection of a proper hood size and the effects of the boundary conditions established by the hood on the low-speed subsonic flow are of concern. For example, with a variation of the technique involving an outflow of the product gases from the top instead of the bottom of the hood, Beyler [17] observed a large change in the measured entrainment rates.

We measured the velocity vectors in the fire-induced flow field [1,3,19] to obtain air entrainment rates. Flow rates across any desired surface were calculated using the velocity vectors if the local density was known. Thomas et al. [18] discussed the possibility of such a quantitative measurement based on their early work that resulted in qualitative information. For surfaces sufficiently far away from the high temperatures we used the ambient density.

Velocity field measurements are useful in the evaluation and calibration of numerical simulations of the fire-induced flow field [3,20–22]. Due to the extreme sensitivity of the fire-induced flow field to boundary conditions [3,22], only calibrated numerical simulations can provide a general purpose methodology for the evaluation of entrainment rates. In Ref. 1, we reported laser doppler velocimetry (LDV) measurements of the velocity field surrounding a 7.1-cm toluene fire. The LDV data provided converged statistical information regarding the probability density functions (PDFs) of the fire-induced velocity showing large fluctuations and both radially inward and outward flows. The measurements for one fire required a 1-year period [1].

A recent planar velocimetry technique called particle imaging velocimetry (PIV) allows significantly faster collection of the velocity field data. One hundred planar images are sufficient to provide information concerning mean entrainment rates and velocity field, which are of primary engineering interest. In the following, we report PIV-based measurements of air entrainment by six fires correlated using the nondimensional parameters of Ref. 2. We also use detailed velocity data for a 30-cm toluene fire as a representative case to demonstrate the strengths and weaknesses of a fire-induced flow analysis [22].

Experimental Methods

Apparatus and Operating Conditions

The two stainless steel burners (15- and 30-cm diameters) are located in the center of a 1.5 × 1.5 × 3-m enclosure. The details of the burner design are identical to those of the burners used by Klassen [23]. The top 1 m of the enclosure is made of glass in order to establish an upper layer as the downstream boundary condition for the fire. The interface between the hot upper layer of combustion products and the ambient air was at 120 ± 3 cm above the fuel surface. Data from five repetitions of measurements for one fire agreed within 15%.

The remaining 2 m of the enclosure are made of a fine wire cloth to protect the fires from ambient disturbances. Background velocity measurements showed that the air was almost quiescent (less than 1 cm/s random velocity) without the pool fire. We checked and matched the exhaust hood opening, interface height, and background velocity before and after each experiment to ensure consistency of boundary conditions for the different experiments.

We considered three fuels (methanol, heptane, and toluene) to obtain data for fires with a range of combustion efficiency, radiative heat loss fractions,

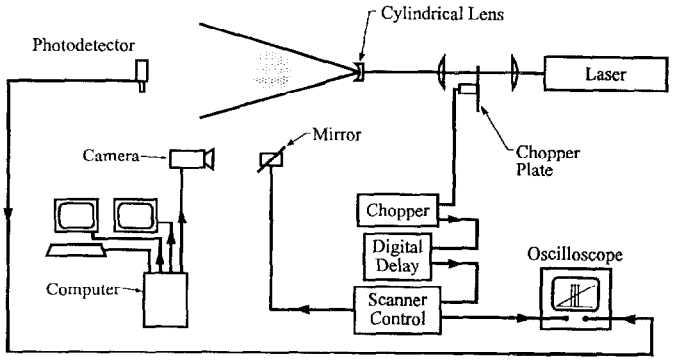

FIG. 1. Schematic configuration of the PIV system.

fire Froude numbers, burning rates, and stoichiometric air requirements as summarized in Table 1. The lip height (the distance from the fuel surface to the burner edge) was 0.5 cm. The burning rates are within 7% of those observed by Klassen [23]. The flame heights (mean value of 60 randomly chosen images in a video record) vary between 32 and 134 cm. The radiative heat loss fractions are rounded-off values from the data of Klassen [23]. The combustion products in the overfire region were sampled using a probe and analyzed using gas chromatography. The combustion efficiencies of heptane and toluene were estimated based on measurements of CO_2 and CO concentrations and soot, and on CO_2 and CO generation factor relationships from Köylü and Faeth [24].

Particle Imaging Velocimetry

The PIV system is shown schematically in Fig. 1. A CW argon-ion laser with multiline power output of 12 W generates a train of dual pulses of light in conjunction with a two-slot (at an angle of 15°) chopper plate rotating at a frequency of 100 Hz. Two convex lenses focus the laser beam at the location of the chopper plate and maximize the signal-to-noise ratio. A cylindrical lens spreads the pulsed laser beams into a light sheet of 2-mm thickness to illuminate a planar section of the flow field for two closely spaced, short time intervals. A bank of cyclone seeders with a fluidized bed seed the air inside the enclosure with Al_2O_3 particles of 0.5-μm mean diameter. A 1.4-MB Kodak CCD camera and a frame grabber capture the light scattered from the seeding particles in the view region during the two laser pulses. To eliminate the directional ambiguity, a scanning mirror introduces a shift in the direction of the mean velocity. A digital delay generator synchronizes the chopper and the scanning mirror. The shift is larger in magnitude than the maximum reverse flow velocity leading to a correct ordering of the two exposures. We process the double-exposure images with a resolution box of the size 32 × 32 pixels (corresponding to 3.5 × 3.5 mm in the flow field). We subtract the velocity shift from the resolved vector field at the analysis stage.

The resulting uncertainty in velocity is less than 2% based on a maximum velocity of 20 cm/s according to the estimation method of Adrian [25]. The PIV measurements of the velocities around a 7.1-cm toluene fire were within 10% of the LDV measurements reported in Ref. 1. We obtained the mean velocity field by averaging 100 instantaneous vector plots representing samples from a 1-h period. That the mean velocities based on 30 images and 100 images agree within 10% justifies the number of samples.

Theoretical Methods

The theoretical analyses follow those in Refs. 3 and 22 with emphasis on the flow induced by a pool fire without a floor. Baum and McCaffrey [22] decomposed entrainment flow velocity V° into two components, namely, the irrotational velocity $\bar{V}^\circ$ and the incompressible velocity $\tilde{V}^\circ$. The irrotational velocity field is the divergence of a potential function ϕ°, and the incompressible velocity field is the curl of a stream function ψ°:

$$\bar{V}^\circ = \frac{\partial \phi^\circ}{\partial z^\circ}\hat{e}_z + \frac{\partial \phi^\circ}{\partial r^\circ}\hat{e}_r$$

$$\tilde{V}^\circ = \frac{1}{r^\circ}\frac{\partial \psi^\circ}{\partial r^\circ}\hat{e}_z - \frac{1}{r^\circ}\frac{\partial \psi^\circ}{\partial z^\circ}\hat{e}_r \qquad (1)$$

where the superscript $^\circ$ indicates a dimensional quantity. Following the nondimensionalization of Ref. 22 and representing the resulting nondimensional quantities with identical symbols without the asterisk, we write the governing equations in a nondimensional, axisymmetric, cylindrical coordinate system as

$$\frac{\partial^2 \phi}{\partial z^2} + \frac{1}{r}\frac{\partial}{\partial r}\left(r\frac{\partial \phi}{\partial r}\right) = Q(\mathbf{r}) \qquad (2)$$

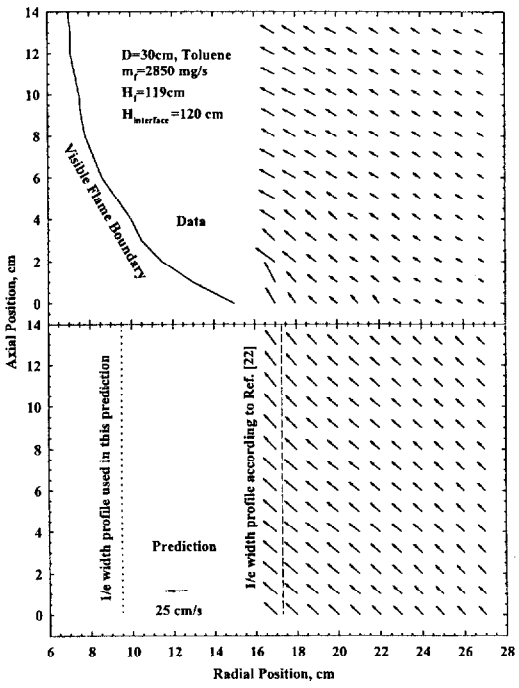

FIG. 2. Measurements and prediction of mean velocity vectors around a 30-cm toluene pool fire.

$$\frac{\partial^2\psi}{\partial z^2} + \frac{\partial^2\psi}{\partial r^2} - \frac{1}{r}\frac{\partial\psi}{\partial r} = -r\omega_\theta(\mathbf{r}) \tag{3}$$

As in Ref. 22, we estimate the nondimensional source terms in the two equations, $Q(\mathbf{r})$ (heat release rate) and $\omega_\theta(\mathbf{r})$ (baroclinic vorticity) using the correlations of buoyant diffusion flame structure given by McCaffrey [26]. Gaussian profiles are assumed for radial distribution of both velocity and excess temperature. The Gaussian profiles for temperature and velocity distributions are characterized by the radius of the point at which the velocity reaches a value equal to $1/e$ of that at the centerline. The use of the value for this radius given in McCaffrey [26] led to a substantial overprediction of the fire-induced velocity at all points. Since heat release rate and vorticity distribution data for the present fires are not available, the radius for the $1/e$ point was adjusted using a single ad hoc constant defined in the following section.

The boundary conditions along the centerline (as in Ref. 3) are

$$\frac{\partial\phi}{\partial r} = 0,\ \psi = 0 \text{ at } r = 0, \text{ for all } z \tag{4}$$

The boundary conditions for the velocity potential at the outer edge of computational domain are taken to be equal to those of a potential flow caused by an equivalent normalized point heat source of strength $(1 - X_R)$, where X_R is the radiative heat loss fraction:

$$\phi = \frac{1 - X_R}{4\pi\sqrt{r^2 + z^2}} \tag{5}$$

The boundary values of the stream function are obtained as the solution of an ordinary differential equation in the spherical coordinate system resulting from a coordinate transformation of Eq. (3), following Ref. 22. Substituting $\psi = \rho^{5/3}F(\mu)$, where $\rho = \sqrt{r^2 + z^2}$, $\mu = \cos\theta$, where θ is the polar angle, into Eq. (3) yields

$$\frac{d^2F}{d\mu^2} + \frac{10F}{9(1 - \mu^2)} = \Omega(\mu) \tag{6}$$

where $\Omega(\mu)$ is the normalized vorticity. Along the centerline, μ is equal to unity for locations above the fuel surface and equal to -1 for locations below the fuel surface. The stream function is zero at both locations:

$$F(-1) = F(1) = 0 \tag{7}$$

Equations (2) and (3) are solved using a finite difference method subject to the boundary conditions discussed above and the distributions of volumetric heat release rates and azimuthal vorticity given in [22]. The stream function yields the solenoidal velocity field $\vec{V}$, and the velocity potential yields the irrotational expansion field $\vec{V}$. The entrainment velocity field is the sum of these two portions.

Results and Discussion

The upper half of Fig. 2 represents the mean entrainment flow field around the 30-cm toluene pool fire. The vectors represent the mean convection velocities. Also shown in the figure is an instantaneous visible flame boundary. Large vertical velocity components at the elevation of the fuel surface, at radii larger than that of the pool edge, show that considerable air is entrained from regions below the elevation of the fuel surface. The velocity vectors shown in Fig. 2 have a significantly different orientation than the horizontal vectors observed for the 7.1-cm toluene pool fire with a floor [1]. These dramatic differences in the velocity patterns support the prediction of Walker and Moss [27]. At a given height, both axial and radial velocities increase with smaller radial distance from the flame, and at a given radial location, the velocity only changes slightly with the axial distance. At the farthest radial location ($r = 27$ cm), the vertical velocity component is comparable to the radial velocity component.

The correlations for heat release rate and vorticity distributions given in Ref. 26 require that the radius of the $1/e$ point in the velocity profile be approximately 17.5 cm as shown in the bottom half of Fig.

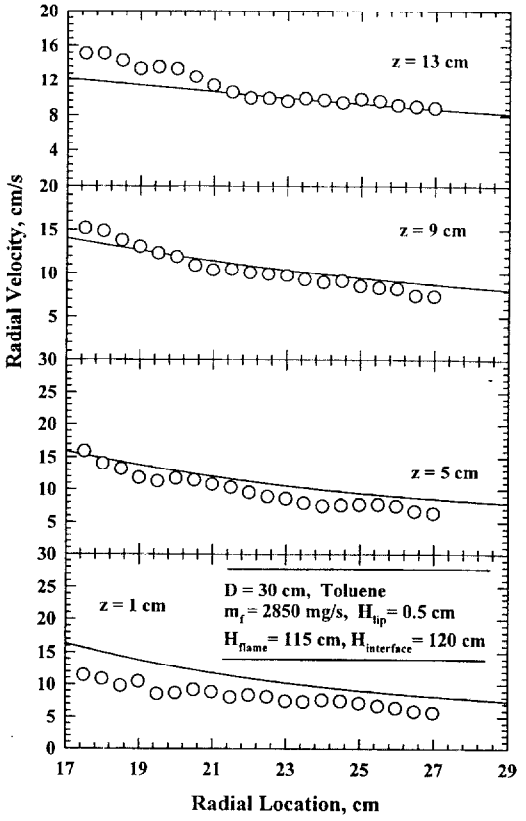

FIG. 3. Measurements and predictions of radial velocities around a 30-cm toluene pool fire at two different heights.

2. With these correlations, a substantial overprediction of both the radial and the axial velocity components was observed. Since the vorticity and heat release rate data for the present fire are not available, a reduction in the radius of the 1/*e* point in the velocity profile to 9.5 cm was utilized. The resulting predictions of velocity vectors are shown in the bottom half of Fig. 2. These are in reasonable qualitative and quantitative agreement with the measurements. The discrepancies between the measurements and predictions in Fig. 2 are mainly in the vertical velocity component. The measurements and predictions of radial profiles of radial velocities at four axial stations are shown in Fig. 3. These also show very encouraging agreement with the predictions generally within 20% of the measurements, except at the 1-cm position. As discussed in Ref. 3, the volumetric heat release rate distribution and the vorticity distribution need to be measured for conditions representative of the present fires.

Mass flow rate into a cylindrical surface with a radius 1 cm larger than the radius of the individual pool burners is calculated based on the mean velocity fields for the six pool fires. This choice of the interface represents a specific location independent of the variations in the flow field and is outside the visible flame interface at all times. In lumped-parameter analyses typical of fire safety codes, this interface can be defined in an exact manner for specifying the air entrainment rate into the cylindrical control volume of interest. Thomas et al. [18] also identified a cylindrical surface of a certain radius greater than that of the pool as a realistic interface. Ambient air density is used in calculation of mass flow rate because thermocouple measurements show that at a radial location 1 cm larger than the pool radius, the temperatures are less than 10 K higher than the ambient temperature. The air mass flow rate entrained up to a height "m_{ent}" is nondimensionalized using the product mass flow rate of stoichiometric combustion $(S + 1)\,\dot{m}_f$. The Froude number is the ratio of the inertia to buoyancy forces, and Delichatsios [2] showed that with appropriate approximations concerning velocity and length scales, the fire Froude number can be calculated as

$$Fr_f = \frac{\dot{m}_f \Delta H_c}{\rho_\infty [\Delta H_c/(S+1)] D^2 \sqrt{[\Delta H_c/[(S+1)C_p T_\infty]] g D (X_A - X_R)}} \quad (8)$$

where $\dot{m}_f$ is the burning rate, ΔH_c is the heat of combustion, ρ_∞ is the ambient density, S is the ratio of air to fuel mass at stoichiometric condition, D is the pool diameter, C_p is the constant specific heat of gases, T_∞ is the ambient temperature, and g is the gravitational acceleration. Zhou et al. [28] obtained the fire Froude number as the parameter using the governing equations with the velocity and length scales defined by Delichatsios [2]. The combustion efficiency X_A and radiative heat loss fractions X_R required for the calculation of Fr_f are listed in Table 1. The entrainment rate data are plotted as a function of nondimensional distance above the fuel surface in Fig. 4. Error bars represent measurement uncertainty based on repeated data. An excellent collapse of measured normalized entrainment rates for the six fires is observed. A best-fit correlation of the normalized entrainment rates with Z/D, normalized axial distance, is shown in Fig. 4. The correlation due to Delichatsios [2] was used in Ref. 1, and reasonable agreement was observed. However, due to the difficulties associated with matching the interfaces between the present data (a cylindrical surface of fixed diameter) and the data upon which the correlations in Ref. 2 (unknown implicit surface) were based, the latter are not shown in Fig. 4. The collapse of data from six different fires confirms the validity of using the fire Froude number as the relevant nondimensional parameter.

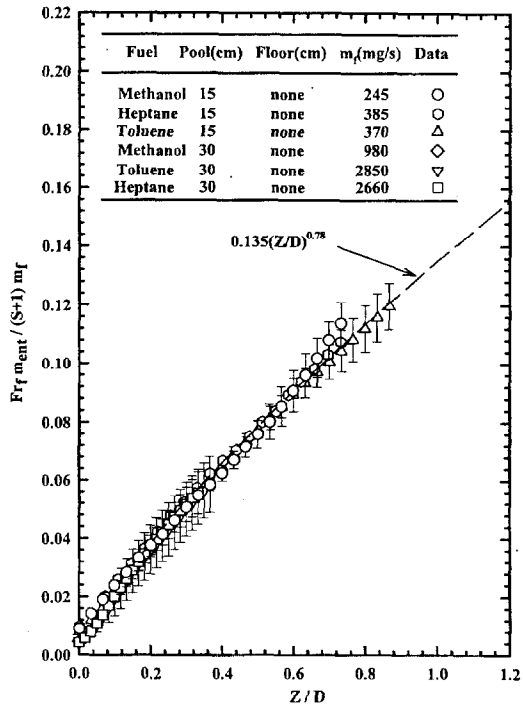

FIG. 4. Normalized entrainment rates for six fires as a function of normalized axial distance.

Conclusions

1. PIV measurements of the fire-induced flow field can be used to obtain the entrainment rates of pool fires.
2. The collapse of the normalized entrainment rate data with the fire Froude number as the parameter as a function of the normalized distance from the fuel surface confirms that the fire Froude number is an appropriate nondimensional parameter for correlating pool fire entrainment data.
3. Use of existing correlations for heat release rate and vorticity distributions in conjunction with an existing kinematic analysis results in an overprediction of the fire-induced velocity field. However, significantly improved predictions were obtained using a single constant used for reduction of the 1/*e* radius in the heat release rate and vorticity distributions.
4. More accurate, experimentally verified heat release rate and vorticity distributions are needed to improve predictions of the fire-induced flow.

Acknowledgments

The research was supported by the Center for Fire Research, Building and Fire Research Laboratory, National Institute of Standards and Technology under Grant No. 60NANB2D1291 with Drs. Anthony Hamins and Takashi Kashiwagi serving as NIST Scientific Officers.

REFERENCES

1. Zhou, X. C. and Gore, J. P., *Combust. Flame* 100:52–60 (1995).
2. Delichatsios, M. A., *Combust. Flame* 70:33–46 (1987).
3. Zhou, X. C., Gore, J. P., and Baum, H. R., *Central States/Western States Joint Meeting of the Combustion Institute*, San Antonio, TX, April 23–26, 1995.
4. McCaffrey, B. J., National Bureau of Standards (currently NIST) Report No. NBSIR 79-1910, 1979.
5. Cox, G. and Chitty, R., *Combust. Flame* 39:191–209 (1980).
6. McCaffrey, B. J. and Cox, G., National Bureau of Standards (currently NIST) Report No. NBSIR 82-2473, 1982.
7. Yumoto, T. and Koseki, H., *Fire Sci. Technol.* 2:91–97 (1982).
8. Koseki, H. and Yumoto, T., *Fire Technol.* Feb:33–47 (1988).
9. Weckman, E. J., *Heat Transfer Phenomena in Radiation, Combustion and Fires, HTD-Vol. 106*, ASME, NY, 1989.
10. Ricou, F. P. and Spalding, D. B., *J. Fluid Mech.* 11:21–32 (1961).
11. Delichatsios, M. A. and Orloff, L., *Twentieth Symposium (International) on Combustion*, The Combustion Institute, Pittsburgh, 1984, pp. 367–375.
12. Zukoski, E. E., Kubota, T., and Cetegen, B. M., *Fire Safety J.* 3:107–121 (1980/81).
13. Cetegen, B. M., Zukoski, E. E., and Kubota, T., National Bureau of Standards (currently NIST) Report No. NBS-GCR-82-402, 1982.
14. Cetegen, B. M., Zukoski, E. E., and Kubota, T., *Combust. Sci. Technol.*, 39:305–331 (1984).
15. Toner, S. J., Zukoski, E. E., and Kubota, T., National Bureau of Standards (currently NIST) Report No. NBS-GCR-87-528, 1987.
16. Zukoski, E. E., *Fire Safety Science—Proceedings of the Fourth International Symposium*, 1994.
17. Beyler, C. L., Ph.D. Thesis, Harvard University, Cambridge, MA, 1983.
18. Thomas, P. H., Baldwin, R., and Heselden, A. J., *Tenth Symposium (International) on Combustion*, The Combustion Institute, Pittsburgh, 1965, pp. 983–996.
19. Zhou, X. C. and Gore, J. P., *ASME Winter Annual Meeting Session of Fire and Combustion Systems*, Chicago, IL, November 1994.
20. Taylor, G. I., *J. Aero/Space Sci.* July:464–465 (1958).
21. Morton, B. R., *Tenth Symposium (International) on Combustion*, The Combustion Institute, Pittsburgh, 1965, pp. 973–982.
22. Baum, H. R. and McCaffrey, B. J., *Fire Safety Science—Proceedings of the Second International Symposium*, Tokyo, Japan, 1988.

23. Klassen, M., Ph.D. Thesis, The University of Maryland, College Park, MD, 1992.
24. Köylü, Ü. Ö. and Faeth, G. M., *Combust. Flame* 87:61–76 (1991).
25. Adrian, R. J., *Int. J. Heat Fluid Flow* 7:127–145 (1986).
26. McCaffrey, B. J., *Combust. Flame* 52:149–167 (1983).
27. Walker, N. L. and Moss, J. B., *Combust. Sci. Technol.* 41:43–53 (1984).
28. Zhou, X. C., Gore, J. P., and Baum, H. R., *Proceedings of the Central States Meeting of the Combustion Institute, St. Louis, MO,* May 5–7, 1996.

COMMENTS

Howard D. Ross, NASA Lewis Research Center, USA. Did you see particles swept beneath the visible flame into the core? How did you introduce particles into the flow?

Author's Reply. We saw particles being entrained across the visibly attached flame surface near the pool edge. We created a cloud of almost quiescent particles in the entire enclosure using an ultralow velocity seeder that utilizes a combination of fluidization and cyclone seeding concepts.